PHYSICAL REVIEW FLUIDS **2**, 100503 (2017)

Transport of particles, drops, and small organisms in density stratified fluids

Arezoo M. Ardekani,[1,*] Amin Doostmohammadi,[2] and Nikhil Desai[1]
[1]*School of Mechanical Engineering, Purdue University, West Lafayette, Indiana 47907, USA*
[2]*Rudolf Peierls Centre for Theoretical Physics, University of Oxford, Oxford OX1 3NP, United Kingdom*
(Received 13 June 2017; published 17 October 2017)

Sedimenting particles and motile organisms are ubiquitously found in oceans and lakes, where density stratification naturally occurs due to temperature or salinity gradients. We explore the effects of stratification on the fundamental hydrodynamics of settling particles, rising drops, and small organisms. The results of our direct numerical simulations of the sedimentation of particles show that the presence of vertical density gradients in the water column can substantially affect the settling dynamics of a particle, interaction between a pair of particles, and settling rates and microstructure of suspension of particles. We show that elongation of particles affects both the settling orientation and the settling rate of particles in stratified fluids, which will have direct consequences on the vertical flux of particulate matter and carbon flux in the ocean. We further demonstrate an unexpected effect of buoyancy, potentially affecting a broad range of processes at pycnoclines in oceans and lakes. In particular, stratification has a major effect on the flow field, energy expenditure, and nutrient uptake of small organisms. In addition, the role of stratification in pattern formation of bioconvection plumes of algal cells and in biogenic mixing is investigated. In particular, the numerical approach allows for considering the effects of background turbulence and hydrodynamic perturbations produced by swimming organisms, shedding light on the contribution of organisms in the mixing process in aqueous environments.

DOI: 10.1103/PhysRevFluids.2.100503

I. INTRODUCTION

Density stratification—due to salinity and/or temperature gradients—is a characteristic feature of aquatic systems ranging from ponds to oceans [1,2]. The layers, $O \sim 1-1000$ m in length, across which there is a sharp change in the water density are called "pycnoclines." These pycnoclines are associated with intense biological activity (e.g., formation of algal blooms) and directly impact carbon fluxes into the ocean by inhibiting the descent of marine snow particles (aggregates > 0.5 mm in diameter) [3]. An increase in the vertical density stratification due to the climatic changes [4] promotes further accumulation of marine snow [3] and, consequently, the formation of phytoplankton blooms [5]. The latter leads to enhanced sequestration of carbon dioxide as the phytoplankton in the ocean surface consume dissolved CO_2 for photosynthesis, and some of them sink to the ocean bed when they die. This "biological pump" is responsible for transferring about 300 million tons of carbon from the atmosphere to the oceans every year [6,7].

Algal blooms formed in freshwater systems are detrimental, and they are known to significantly disrupt water supply systems [8]. On an ecological level, harmful algal blooms (HABs) have an adverse effect on the coastal biota. Toxins released from unicellular marine algae (e.g., dinoflagellates and diatoms) accumulate in the tissues of fish and invertebrates [9,10], resulting in marine organism mortalities and fish kill. Density stratification acutely affects algal bloom formation [3,8,11], leading to low dissolved oxygen levels, and food web disruption. Events such as a sudden rain storm, discharge of submarine, and freshwater runoff from rivers can affect the formation of bioluminescent plankton blooms and harmful algal blooms [12,13], concomitantly affecting hydrodynamic, acoustic, and optical performances of sea platforms [14]. The aforementioned environmental consequences

*ardekani@purdue.edu

make it imperative to develop a fundamental understanding of transport, and accumulation, of particles and organisms in density stratified fluids.

In spite of the widespread implications of stratification on the swimming of microorganisms and settling of particles, the underlying hydrodynamic intricacies remain poorly understood. In oceans and lakes, the ambient fluid density varies on a length scale of $L_\rho = \Delta\rho_0/\gamma \sim O(1)$ in meters, where $\Delta\rho_0$ is a reference density variation (e.g., 27 kg m^{-3}) and γ (0–2 kg m^{-4}) is the vertical gradient in fluid density. This length scale is much larger than the characteristic size of the marine organisms and particles (in the range of micrometers to centimeters). However, it has been recently shown that the appropriate length scale for incorporating density variation effects is $L_s = (\mu\kappa/\gamma g)^{1/4}$, where μ is the dynamic viscosity of water, κ the diffusivity of the stratifying agent, and g the acceleration due to gravity [15]. This length scale has been previously introduced in a different context (diffusion induced flows along inclines in a stably stratified fluid) by Phillips [16]. Importantly, typical values of γ show that L_s is often as small as a fraction of a millimeter (hence $L_s \ll L_\rho$), thus overturning the notion that the fluid mechanics of aquatic organisms and small particles is unaffected by stratification.

The presence of a density gradient leads to significant modifications in the flow physics as a particle settles, or an organism swims, through the stratified fluid. In a homogeneous fluid with kinematic viscosity ν, the motion of a particle or organism of characteristic length L and characteristic velocity W_p is well described by the Reynolds number, $\mathrm{Re} = W_p L/\nu$. In a stratified fluid, the buoyancy force and the diffusivity of the stratifying agent are also important. The buoyancy force is represented by the Froude number, $\mathrm{Fr} = W_p/(NL)$, where $N = (\gamma g/\rho_0)^{1/2}$ is the Brunt-Väisälä frequency, the natural frequency of oscillation of a vertically displaced fluid particle in a stratified fluid. Moreover, the difference between the momentum diffusivity and the diffusivity of the stratifying agent κ impacts the settling of particles or swimming of organisms in stratified fluids and their ratio can be characterized by the Prandtl number, $\mathrm{Pr} = \nu/\kappa$. The list of dimensionless parameters are given in Table I. In addition to introducing new dimensionless groups, stratification causes major qualitative differences in flows in the vertical and horizontal directions. The horizontal flows of stratified fluids have been extensively studied [17–19] and the drag reduction due to internal waves is well understood [20,21]. Spherical particles settling through sharp density interfaces show an increase in their drag coefficient [22–25]. Our recent studies have explored the flow fields of organisms and dynamics of particles swimming or settling in stratified fluids. The present paper discusses the fluid mechanics governing transport of organisms and particles in the context of the following questions:

(a) How does stratification influence sedimenting particles, rising drops, and swimming organisms?

(b) Does density stratification lead to enhanced clustering in a suspension of particles, drops, and organisms?

(c) How does elongation of particles modify their motion in a stratified water column?

(d) What is the role of density stratification on bioconvection plumes in a suspension of algal cells?

(e) To what extent do swimming organisms contribute to biogenic mixing in stratified oceanic environments?

These questions are addressed by investigating the role of stratification in the suspension of particles and organisms by utilizing three-dimensional fully resolved computational fluid dynamics tools. In Sec. II, governing equations, relevant dimensionless parameters, and the computational framework based on a semianalytic approach and direct numerical simulation (DNS) are introduced. In Sec. III, results of the fully resolved, three-dimensional DNS of the unsteady settling of rigid and deformable drops in stratified fluids are provided. Settling dynamics are discussed for individual particles, pairs of interacting particles, and suspension of particles, and new mechanisms for aggregation of particles in the presence of background density gradient are introduced. Moreover, one aspect of geometrical complexity is addressed by characterizing the effect of elongation of particles on settling dynamics in a density stratified fluid. In Sec. IV, the results of modeling the full nonlinear effects of stratification on motility are presented and it is shown that a frequent feature

TABLE I. List of dimensionless parameters important in the study of settling particles and droplets in stratified fluids. Here, ρ_p denotes particle density and d is the particle diameter, ρ_0 is a reference density of the background fluid, μ is the dynamic viscosity of the fluid, ν is the kinematic viscosity, κ is the diffusivity of the stratifying agent, g is the gravitational acceleration, and $N = (\gamma g/\rho_0)^{1/2}$ is the Brunt-Väisälä frequency. In the case of multiparticle systems, N_p denotes the number of particles and L is the system size.

Dimensionless number	Definition	Description
Reynolds number, Re	$\rho_0 W_p d_p/\mu$	Ratio of inertial to viscous forces
Froude number, Fr	$W_p d_p/N$	Ratio of inertial to buoyancy forces
Richardson number, Ri	$\rho_0 N^2 d_p^3/(\mu W_p)$	Ratio of buoyancy to viscous forces
Prandtl number, Pr	ν/κ	Ratio of momentum diffusivity to the diffusivity of a stratifying agent
Density ratio, η	ρ_p/ρ_0	Ratio of particle density to the reference density of the fluid
Archimedes number, Ar	$\rho_0 g d_p^3(\rho_p - \rho_0)/\mu^2$	Ratio of gravitational to viscous forces
Volume fraction, ϕ	$N_p \pi d_p^3/(6L^3)$	Fraction of the domain occupied by particles

of the physical environment—density stratification—can have direct ecological consequences on motility-related traits, including energy expenditure, nutrient uptake, and predator-prey interaction. Furthermore, stratification impact on bioconvection plumes of algal cells and biogenic mixing induced by swimming organisms in the presence of background turbulence are investigated. Finally, in Sec. V, concluding remarks and future directions are discussed.

II. GOVERNING EQUATIONS

The vast majority of organisms and particles being considered in our studies are "small" (micrometers to centimeters), and their motion is predominantly in the viscous flow regime. The prevalence of small particles is apparent from the observations of particle size spectra [26], which show that the abundance of marine particles and organisms scales with the inverse of their size to the fourth power. Even then, the basics of particle and organism motion (and/or accumulation) in the presence of density stratification have been marginally explored from a fluid dynamics perspective, thus calling for fundamental research in this topic. In this section, we discuss both a semianalytical approach, based on point-force singularities, and fully resolved simulation techniques to accurately capture the physics of the stratification impact on the settling of particles and swimming of marine organisms in environmentally relevant setups.

The equations governing the fluid motion under the Boussinesq approximation are

$$\nabla \cdot \mathbf{u} = 0, \tag{1}$$

$$\rho_0 \frac{\partial \mathbf{u}}{\partial t} + \rho_0 \mathbf{u} \cdot \nabla \mathbf{u} = -\nabla p + \mu \nabla^2 \mathbf{u} + \rho \mathbf{g} + \mathbf{f}_b, \tag{2}$$

$$\frac{\partial T}{\partial t} + \mathbf{u} \cdot \nabla T = \kappa \nabla^2 T, \tag{3}$$

where $\mathbf{u} = (u, v, w)$ is the velocity field, t is time, p is the pressure, ρ is the fluid density, $\mathbf{g} = -g\,\hat{\boldsymbol{k}}$ is the acceleration of gravity, with $\hat{\boldsymbol{k}}$ the vertical unit vector, positive upwards, and $\mathbf{f}_b$ is an external body force. The first equation states that the fluid is incompressible. The second equation expresses conservation of momentum, under the assumption that the effect of variations in fluid density is only considered in the body force $\rho\mathbf{g}$ (Boussinesq approximation). The last equation describes how temperature/salinity changes due to advection and diffusion of the stratifying agent.

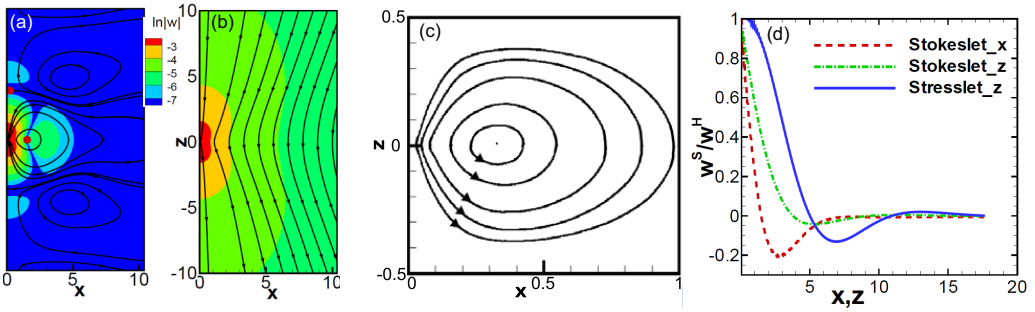

FIG. 1. Stratification dramatically alters flow fields of point-force singularities. A vertical point force is shown (a) in a stratified fluid, (b) in a homogeneous fluid, and (c) between two horizontal walls. Black lines are streamlines; colors indicate the magnitude of vertical velocity, w. (d) The results show that stratification induces a sharper decay of fluid velocity, w^S, with distance from the disturbance compared to the homogeneous fluid, for both a Stokeslet (red, green) and a stresslet (blue). (Reprinted from [15] with the permission of APS Publishing.)

Equations (2) and (3) are coupled as the fluid density is related to the temperature variation by $\rho = \rho_0(1 - \alpha T)$, where α is the thermal expansion coefficient and ρ_0 is the reference density of the fluid, chosen as the density of the background fluid at the initial location of the particle. It should be noted that the same governing equations apply to salt stratified fluids. In that case, T, κ, and α represent the salt concentration, diffusivity, and salinity contraction coefficient, respectively.

A. Fundamental singularities in a stratified fluid

The far-field velocity generated by a settling particle and a motile organism in the $\mathrm{Re} = 0$ limit can be described by the point-force singularities, a "Stokeslet" and a "stresslet," respectively. Here, we consider steady viscous flow induced in a vertically stratified fluid by a point force $\mathbf{f}$. In this case the external body force in Eq. (2) is $\mathbf{f}_b = \mathbf{f}\delta(\mathbf{r})$, and inertial terms are neglected. The resulting linearized equations can be solved analytically in Fourier space after linearization, followed by numerical inversion to recover the solution in the real space [27]. The details of fundamental low-Re singularity solutions of the flow induced by a point force and a force dipole are shown in Ref. [15]. These semianalytical solutions hold for small isopycnal deflections and do not account for the nonlinear convection term in the transport equation.

The semianalytical results reveal that stratification dramatically alters the flow field generated by a point force (Stokeslet) by creating toroidal eddies [Fig. 1(a)], which stand in stark contrast to the monodirectional flow of a Stokeslet in a homogeneous fluid [Fig. 1(b)]. This is due to the suppression of the vertical motion of the fluid, which leads to the formation of recirculation patterns. Eddy formation is consistent with the tendency of stratification to hinder vertical motion, as highlighted by comparing the recirculating patterns formed due to stratification with the case where stratification is replaced by two horizontal walls. In the latter case, a qualitatively similar eddy occurs due to the confinement (Fig. 1(c); see also [28]).

Point-force singularities only provide information about the far-field flow generated by a moving particle and swimming organism in small-Reynolds- and Péclet-number regimes, whereas a full description requires numerical solution of the nonlinear equations. To this end, Ardekani and co-workers have developed three-dimensional, fully nonlinear simulations, investigating the motion of a single settling sphere [29], a motile organism [30], an elongated particle [31], and a rising droplet [32], as well as suspensions of particles [33], drops [34], and organisms in multibody systems in the presence of stratification, as well as background turbulence [35]. In this review article, we summarize these studies.

B. Fully resolved numerical simulations

In this section, we discuss the numerical tools that are used to solve the full nonlinear equations of motion to understand the effects of stratification on the motion of suspension of particles and organisms. Ardekani and co-workers have developed advanced numerical tools to study particle motion in viscous fluids [36,37] and extensively tested them against benchmark problems. The code is based on a finite-volume method. The Navier-Stokes equations are solved on a nonuniform staggered grid, using an operator splitting technique. Convection and diffusion terms are discretized using the QUICK (quadratic upstream interpolation for convective kinetics) and central difference schemes, respectively [34,38]. The time evolution is obtained using a second-order Runge-Kutta scheme. Objects of general shape and multiple particles [37] are resolved using a distributed Lagrange multiplier method [39], where the equations of fluid motion are first solved for the entire computational domain including the inside of the particle, and then a rigidity constraint is implemented inside the particle by means of Lagrange multipliers. The details of the projection step and calculation of the rigidifying force are provided in our previous publications [29,37].

The same numerical approach can be applied to self-propelled organisms, for which the kinematics of deformation are specified as an input and the flow field is computed by solving the momentum equation with an added body force $\mathbf{f}_b$ [40], which models the presence of the organism (see below). The density in the inertial terms of the momentum equation would be equal to ρ_p in the "organism domain" and ρ_f in the fluid domain. By defining the body force as

$$\mathbf{f}_b = \mathbf{f}_b^* + C\frac{\rho\phi}{\Delta t}(U_p + \boldsymbol{\omega}_p \times \mathbf{r} + \mathbf{u}_i - \mathbf{u}) \tag{4}$$

inside the organism (and zero elsewhere), we can enforce the organism to move with the desired deformation kinematics, where $\mathbf{f}_b^*$ is the force computed from the previous iteration, C is a dimensional constant (whose value does not affect the final converged solution), and ϕ is an indicator function defined to be $\phi = 1$ inside the particle and $\phi = 0$ outside. The velocity field inside the organism is decomposed into a velocity due to the rigid body motion of the organism, $\mathbf{u}_p$, plus a solenoidal velocity, $\mathbf{u}_i$, imposed inside the swimmer causing its propulsion. The former is calculated as $\mathbf{u}_p = \boldsymbol{U}_p + \boldsymbol{\omega}_p \times \mathbf{r}$, where $\boldsymbol{U}_p$ and $\boldsymbol{\omega}_p$ are the organism translational and angular velocities calculated as [29,40]

$$\boldsymbol{U}_p = \frac{1}{M_p}\int_{V_p} \rho_p(\mathbf{u} - \mathbf{u}_i)\, d\mathbf{V} \quad \text{and} \quad \mathbf{I}_p\boldsymbol{\omega}_p = \int_{V_p} \rho_p \mathbf{r} \times (\mathbf{u} - \mathbf{u}_i)\, d\mathbf{V}, \tag{5}$$

where V_p, M_p, and $\mathbf{I}_p$ are the volume, mass, and moment of inertia of the organism. It is important to mention here that an appropriate choice of $\mathbf{u}_i$ will enable us to model the complex movement of organisms ranging from algae to jellyfish. The details of the computational method are given in recent publications on the suspension of squirmers in a homogeneous fluid [40,41], rod-shaped swimmers [42], and motion of an undulatory flagellated swimmer [43].

III. SETTLING AND RISING OF RIGID PARTICLES AND DEFORMABLE DROPS IN STRATIFIED FLUIDS

A. Individual particles

1. Settling of spherical particles in sharp and continuous stratifications

Gravitational settling of a single particle and droplet has been extensively studied in sharp density gradients [22,44–46]. In particular, it was shown experimentally that a sphere settling through a sharp density interface experiences an order of magnitude larger drag force due to buoyancy effects compared to settling in a homogeneous fluid [22] and that the sphere is subject to long residence times at the sharp interface [44]. In linear stratified fluids, the study of steady state settling motion showed that in both inertial and viscous regimes the drag on the spherical particle significantly increases [23,25]. We have recently conducted numerical simulations of the settling of a rigid sphere in linearly

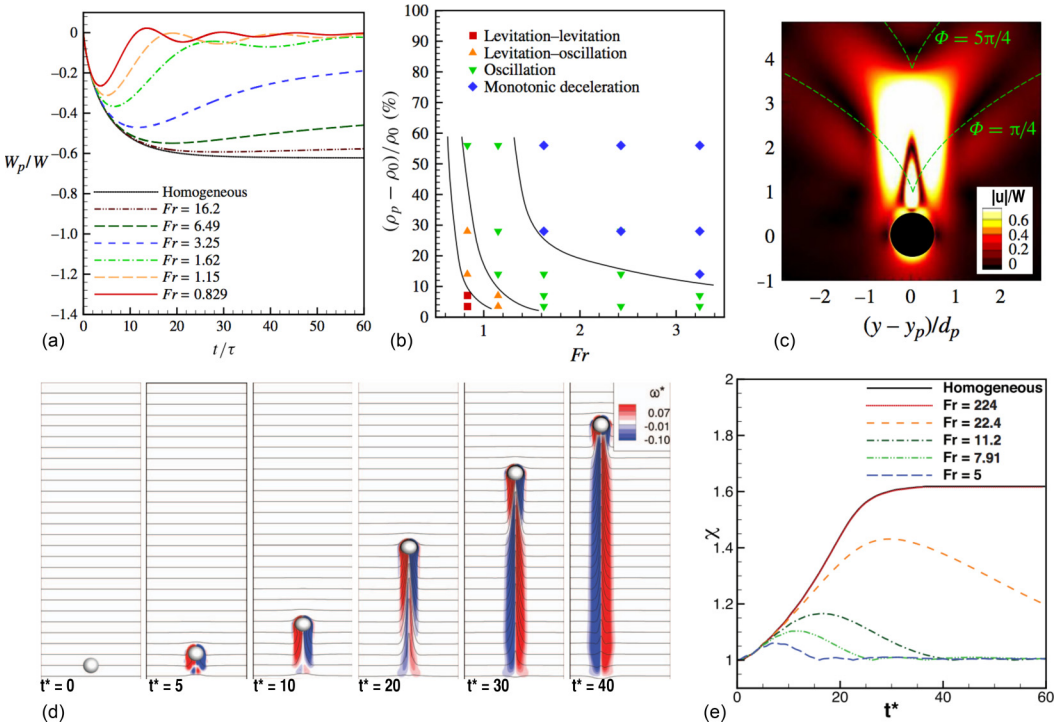

FIG. 2. Settling dynamics of a rigid particle and a deformable drop in linearly stratified fluids for various Froude numbers Fr (smaller Fr corresponds to stronger stratification). (a) The temporal evolution of the settling velocity of a rigid particle for various strengths of the stratification. $\tau = \sqrt{d_p/g}$ denotes the characteristic time and $W = (\rho_p - \rho_0)gd_p^2/(18\mu)$ is the Stokes terminal velocity. (b) A phase diagram of distinct deceleration dynamics. (c) Generation of lee waves around the particle, evident from contours of the velocity magnitude. Green lines show the lines of constant phase calculated from the method of stationary waves. y_p denotes the transverse position of the particle. (d) Rising motion of a deformable drop in a linearly stratified fluid over the course of time ($t^* = t/\tau$). Color maps show dimensionless vorticity $\omega^* = \omega\tau$ contours and solid lines illustrate constant density lines. (e) The effect of stratification on the deformation of a drop. The drop deformation is quantified by $\chi = I_1/I_2$, where I_1 and I_2 are the largest and smallest eigenvalues of the second moment of inertia tensor, with $\chi = 1$ corresponding to a spherical drop. Stronger stratification (smaller Froude number) leads to a more spherical drop ($\chi \sim 1$). [Panels (a)–(c) reprinted from [29] with the permission of Cambridge University Press and (d), (e) reprinted from [32] with the permission of AIP Publishing.)

stratified fluids, investigating the transient dynamics of particle sedimentation. Our simulation results reveal a wealth of dynamics offered by the combination of buoyancy forces and inertial effects on the particle settling under gravity [see Fig. 2(a)] [29]. We report that unlike the settling in a homogeneous fluid, where the particle velocity monotonically increases before reaching a constant settling speed, settling of a particle in stratified fluids shows a maximum in the settling velocity, with the magnitude of this maximum being reduced at stronger stratifications. This suppression of vertical motion is then followed by distinct dynamical behaviors depending on the strength of the stratification: (i) At weak stratifications, after reaching a maximum, the settling velocity drops continuously until the particle stops [Fig. 2(a), blue line]. (ii) Stronger stratifications lead to emergence of oscillations in the particle velocity [Fig. 2(a), light green line]. We found these oscillations to be induced by the formation of primary, secondary, and tertiary vortices behind the particle; such vortex structures around a settling particle are absent in homogeneous fluids. (iii) At even stronger density gradients, oscillation amplitude grows such that the particle stops settling momentarily, *levitates* for a short time, and then reverses its motion [Fig. 2(a), red line]. At this point, the particle experiences monotonic deceleration,

oscillation, or even levitation depending on the strength of the stratification. A classification of the particle's dynamical behavior can be obtained from a phase diagram based on the Froude number and the density ratio [see Fig. 2(b)]. Furthermore, a closer look into the oscillations in the particle settling velocity reveals that the oscillation frequency scales with the Brunt-Väisälä frequency, and lee waves form around the particle [see Fig. 2(c)]. Moreover, recent experiments by Okino *et al.* [47] have examined time-dependent velocity distribution around a sphere settling with constant speed in linearly stratified fluids at moderate Reynolds numbers.

In addition to a rigid particle, we have also studied the rising motion of a deformable drop in linearly stratified fluids [32]. We found that much like the descent of a rigid particle, the ascent of a deformable drop is markedly suppressed by the presence of density stratification, and secondary vortex structures are seen to manifest around the drop [see Fig. 2(d)]. More importantly, stratification effectively hampers the deformation of drops and for strong stratifications a drop remains closely spherical [see Fig. 2(e)]. In addition to rigid particles and deformable drops, the rising motion of bubbles has been recently studied through experiments on sharp density interfaces [48]. It was shown that, depending on the size of the bubble, it can experience straight or zigzag trajectories at the interface leading to stable and unstable drift volumes behind the bubble, potentially impacting the mixing induced by rising bubbles in stratified fluids.

2. The impact of particle elongation

For a long time, the understanding of particle motion in stratified fluids remained limited to the motion of spherical particles but it is known that many marine particles and organisms are not perfectly spherical [49]. In fact, a majority of phytoplankton are spheroid-shaped (aspect ratio $\sim$5) [50], and slender shapes (rods or needles) outnumber shapes such as spheres and disks. The sedimentation of such elongated particles in *homogeneous* fluids has been studied in detail [51–54], but their behavior under stratification remained unexplored or elusive for quite a long time. In the Stokes regime, the orientation of an ellipsoid does not change as it settles in an unbounded quiescent fluid (due to the "reversibility" of the Stokes flow) [55]. Drag anisotropy dictates that the hydrodynamic drag on an ellipsoid settling parallel to its shorter axis is larger than the one descending parallel to the longer axis. This means that the settling rates in Stokes flows are orientation dependent. However, inertial effects significantly modify the settling dynamics—due to upstream wake formation—by causing rotation of the elongated particles as they settle. Thus any ellipsoid that begins descending in a direction parallel to its major axis in an inertial regime, ultimately settles along a direction that is parallel to its minor axis (broadside settling) [54].

For a particle settling at $\mathrm{Re} \ll 1$ in a stratified fluid, we find that the settling dynamics is affected differently. A torque acts on the particle due to the differential buoyancy experienced by its opposite ends [31]. This buoyancy-induced torque can have important consequences on the retention of particles at density interfaces which affects the formation of thin particle layers and algal blooms [2]. Our simulations for the motion of an ellipsoid settling through a sharp density interface are shown in Fig. 3(a). As stratification is increased in the form of a buoyancy jump, the ellipsoid's minor axis aligns with the vertical direction near the interface and then retains its original orientation after crossing the density divide [see Fig. 3(b)]. The results are very different though, for linear stratification. Here the ellipsoid reorients, once again due to stratification effects, but this time it is the major axis that aligns itself with the vertical direction. Thus, depending upon the intensity (density gradient magnitude) and type of stratification (sharp jump vs. continuously varying) we observe qualitatively and quantitatively different settling behaviors of elongated objects.

B. Dynamics of suspensions

While the effects of the density stratification on the reduced settling velocity of a single sphere have gained significant attention in the research community [15,22,25,29,44], the same cannot be said about the settling rates and accumulation trends of a suspension of particles and/or organisms in stratified fluids. This is in part due to the complexity of the problem which involves coupling

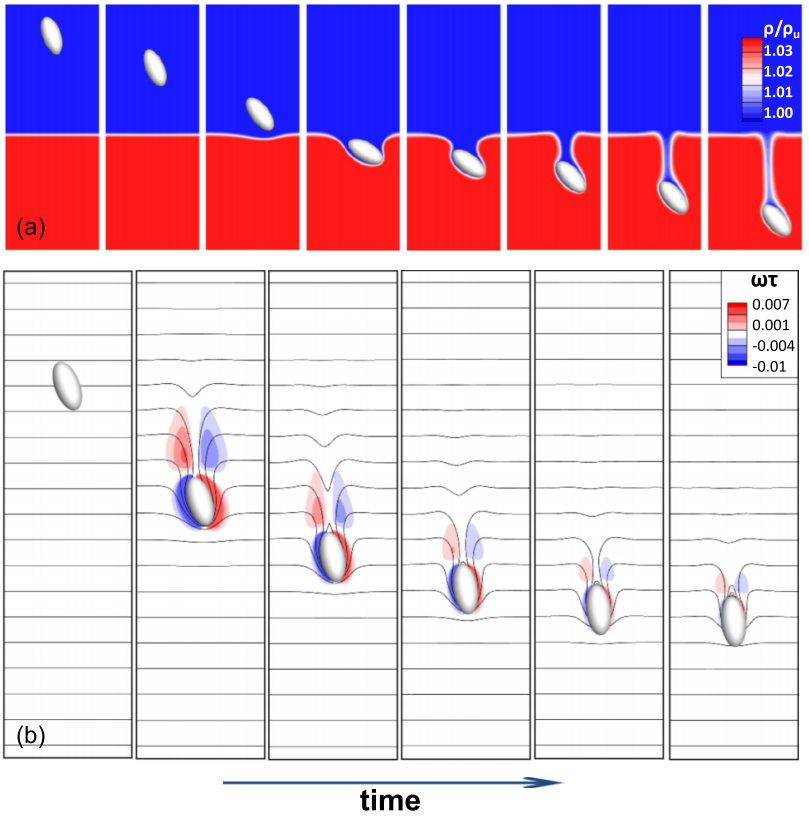

FIG. 3. The settling motion of an ellipsoid at (a) a sharp density interface and (b) a linear stratification. Shown in (a) are the normalized density contours. In (b), the solid lines show the isocontours of density and the color map shows the normalized vorticity contours. (Reprinted from [31] with the permission of APS Publishing.)

between particle-particle hydrodynamic interaction and density stratification. We employed DNS to resolve the motion of particles and organisms and quantify the effect of density stratification on possible cluster formation. We quantified the flow field around a suspension of particles settling in stratified fluids, and provided a correlation between the mean settling velocity of the suspension and the extent of density stratification.

The relative velocity of the particles with respect to the surrounding stratified fluid is represented by the "average slip velocity," $W_s = W_p - \bar{w}_f$, where W_p is the mean velocity of particles averaged over the particle assembly and $\bar{w}_f$ denotes the volume averaged velocity of the fluid phase in the suspension. The normalized slip velocity W_s, when scaled by its homogeneous counterpart W_H, is significantly reduced ($W_s/W_H < 1.0$). The best fit of the data for different volume fractions is obtained as $W_s/W_H = 1 - 61.1\mathrm{Fr}^{-2.07}$. Our results for a swarm of particles in a stratified fluid show that their motion is significantly slowed down, and that they are more aggregated as compared to the same swarm in a homogeneous fluid. We observe a similar behavior (of slower ascent, and an enhanced aggregation) for a swarm of deformable drops ascending in linearly stratified fluids [see Fig. 5(b)] [34]. In fact, the slowing down of a swarm of rising drops can even be predicted by analyzing the motion of a single drop, rising in a stratified fluid. Figure 4 clearly shows the similarity in the time evolution of the instantaneous rise Reynolds numbers for a single drop, and a swarm of drops, for a range of stratifications. It is seen that the rise is substantially slowed down in both cases; however, this effect is much stronger for the swarm of drops. We characterize the microstructure

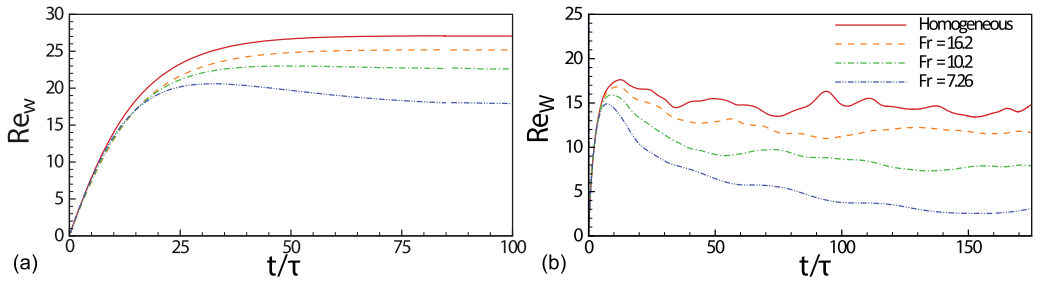

FIG. 4. The time evolution of the instantaneous rise Reynolds number of (a) a single drop and (b) multiple drops in a stratified fluid at different Fr. (Reprinted from [34] with permission of Elsevier.)

of the particle assemblies by comparing the pairwise probability distribution functions (both radial and angular) between homogeneous and stratified fluids. The tendency of horizontal alignment in a suspension of particles or drops is evaluated by measuring the angular pair probability distribution function $G(\theta)$, which quantifies the probability of finding two particles that are oriented at a specific angle with respect to each other, and separated by a prescribed distance r:

$$G(\theta) = \frac{L^3}{N_p(N_p-1)\Delta V(\theta)} \sum_{m=1}^{N_p} \sum_{\substack{n=1,\\ n\neq m}}^{N_p} \delta\left(|r_{mn}| < r; \theta - \frac{1}{2}\Delta\theta \leqslant \theta_{mn} < \theta + \frac{1}{2}\Delta\theta\right), \tag{6}$$

where $\Delta V(\theta) = (2\pi r^3/3)[\cos(\theta - \Delta\theta/2) - \cos(\theta + \Delta\theta/2)]$ is the volume of a spherical sector of radius r, and azimuthal angle θ, between $[\theta - \Delta\theta/2, \theta + \Delta\theta/2]$. Therefore, a higher probability of horizontal clustering will be associated with peaks in the value of $G(\theta)$, observed at angles close to $\theta = \pi/2$. In light of this reasoning, the results shown in Figs. 5(d) and 5(e) illustrate that density stratification leads to the formation of clusters that are predominantly aligned horizontally across the fluid column, both for rigid particles and for a swarm of drops. In addition to peaks around $\theta = \pi/2$, we observe increasingly higher values of $G(0)$ and $G(\pi)$, for reduced Fr, for a suspension of rigid particles [Fig. 5(d)]. All these peaks are "specific to short-range interactions"; i.e., these are only found when $G(\theta)$ is evaluated for $r \sim d$, and are seen to reduce appreciably when $r \geqslant 5d$ (see [33,34] for details). This means that significant vertical (for rigid particles) and horizontal (for rigid particles, and for drops) clustering is observed only at smaller length scales. As opposed to the horizontal configuration ($\theta = \pi/2$), the vertical configurations are unstable. The unstable nature of "short-range vertical interactions" is consistent with our recent study [33] on the interaction of an isolated pair of rigid particles in stratified fluids for both side-by-side and in-tandem configurations. It is interesting to note that the clustering behavior of a suspension can also be deduced by examining the motion of a pair of particles, or drops. A pair of rigid particles sedimenting side-by-side in a stratified fluid are attracted toward each other, after initial repulsion due to inertial effects. This is dramatically different from the side-by-side sedimentation in a homogeneous fluid, where the inertial repulsion persists up to a certain distance after which the rigid particles sediment with an offset in their horizontal separation. The enhanced attraction in a stratified fluid helps explain the higher "short-range" peaks observed at $\theta = \pi/2$ (for lower values of Fr), for the case of a sedimenting suspension of rigid particles. The behavior of particles settling in tandem in a weakly stratified fluid is characterized by *drafting-kissing-tumbling* with a prolonged kissing time and reduced separation as compared to a homogeneous fluid. This regime can change to either *drafting-kissing-separation*, or even *drafting-separation* in stronger background density gradients [57]. There is a noticeable absence of the tumbling behavior. This behavior reinforces the understanding of the more complex response of a suspension of rigid particles, i.e., the existence of peaks at $\theta = 0, \pi$. The dynamics of the particle pair interaction in stratified and homogeneous fluids is summarized in Fig. 5(a). The behavior of an ascending swarm of drops can also be understood by a closer examination of the

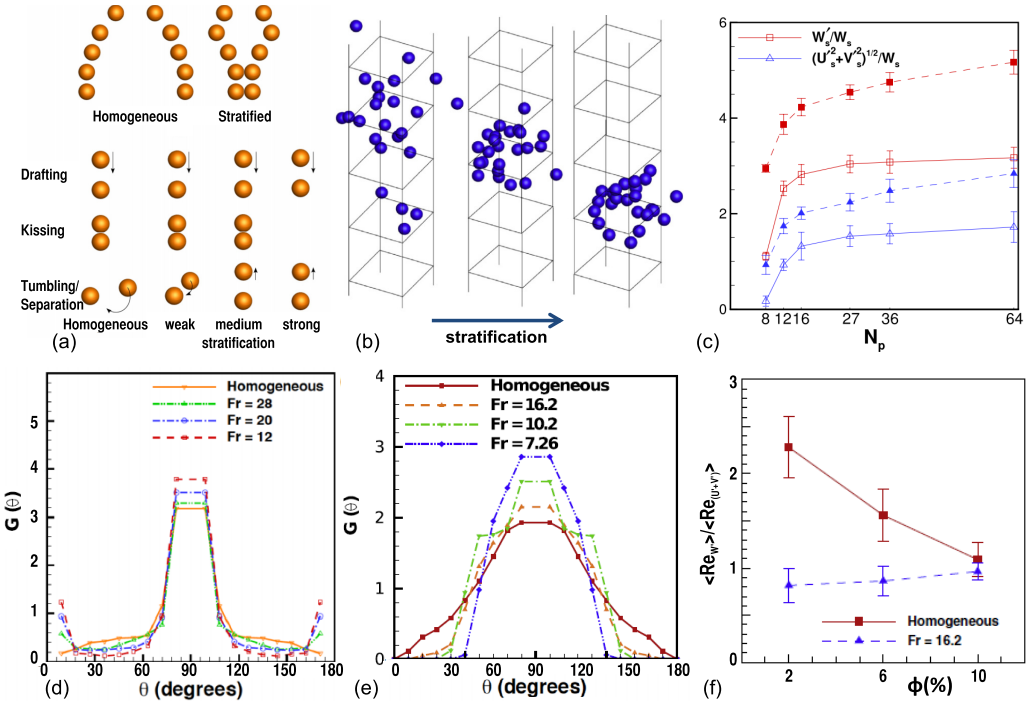

FIG. 5. (a) Schematic of inertial pair-particle interaction in homogeneous and stratified fluids. (b) Dispersion of particles and drops in a stratified fluid is significantly reduced. Left, homogeneous fluid; middle, Fr = 10.2; right, Fr = 7.26. (c) The growth of velocity fluctuations as a function of the system size (number of particles, N_p) is suppressed in a stratified fluid (open symbols) compared to the settling in a homogeneous fluid (solid symbols). Here, W_s denotes the average settling velocity. Stratification leads to a strong horizontal cluster formation in a suspension of (d) particles and (e) drops as shown in plots of angular pair probability distribution function. (f) Density stratification reduces fluctuations in vertical and horizontal velocity components, denoted by $\mathrm{Re}_{W'} = W' d_p/\nu$ and $\mathrm{Re}_{(U'+V')} = (U'+V')d_p/\nu$. (Panels (a), (c), and (d) reprinted from [33] with the permission of AIP Publishing and (b), (e), and (f) reprinted from [34] with the permission of Elsevier.)

motion of two drops rising in a stratified fluid column [58]. We observe that greater stratification leads to an enhanced attraction between two drops ascending side by side, just like it results in higher values of $G(\pi/2)$ for a swarm of drops. The tendency of drops to horizontally cluster in stratified fluids is so high that the vertical configurations become less probable with increased stratification. This is in stark contrast with the behavior of rigid particles, wherein we see higher values of $G(\theta)$ even for $\theta = 0, \pi$.

In addition to the mean settling velocity and the microstructure of a suspension, stratification also impacts the fluctuations in particle velocity. In a homogeneous fluid, there have been several contradictory predictions of the dependence of velocity fluctuations on the system size (system size refers to the *number* of particles for a prescribed volume fraction of the "particle phase") [59]. Our DNS results show that density stratification inhibits both vertical and horizontal velocity fluctuations and suppresses the "growth rate" of fluctuations with increasing system size (compared to the corresponding responses for a homogeneous fluid). This reduction in fluctuations is also apparent in Fig. 4, where we see oscillations of much smaller magnitudes as Fr decreases. Furthermore, even though the *growth rate* of fluctuations reduces progressively with increasing system size [see the slopes of the curves in Fig. 5(c)], the actual *value* of said fluctuations does not seem to saturate, at least for the range of particle numbers considered ($N_p = 8$ to $N_p = 64$) [Fig. 5(c)]. Future studies should investigate the existence of such a "thermodynamic limit" for particle velocity fluctuations

by considering even larger systems. Finally, the velocity fluctuations for a swarm of drops rising in a linearly stratified fluid show drastically different behavior as compared to the homogeneous case [see Fig. 5(f)]. At low volume fractions, velocity fluctuations are more uniformly distributed between vertical and horizontal directions in a linearly stratified fluid ($\langle \mathrm{Re}_{W'} \rangle / \langle \mathrm{Re}_{U'+V'} \rangle$ is closer to unity). This is unlike the anisotropy of the homogeneous fluid case, where fluctuations in the vertical direction are almost twice as intense. The reason behind this enhanced isotropy in stratified fluids can be attributed to the suppression of vertical motion, leading to a uniform energy transfer across the flow. Once again, we stress that this suppression was also seen in the semianalytical results of Sec. II A (Fig. 1) and, therefore, it is important to view the results of more complex systems in light of the fundamental understanding imparted by the simpler problems.

These results hint at intriguing and nontrivial behavior of suspensions in stratified fluids. The dynamics discussed thus far will be even more significantly altered if the particles or drops are replaced by motile organisms. In this case, the self-propulsion of organisms modifies the flow field, leading to altogether different clustering behavior.

IV. HYDRODYNAMICS OF ORGANISMS AT PYCNOCLINES

A. Stratification affects swimming dynamics of a single organism

The impact of planktonic microorganisms on marine ecology is apparent, and well studied [60–63]. However, the same cannot be said about the impact of density stratification on the many fundamental aspects of microorganism motility, their energetic expenditure, and nutrient uptake rates. The first attempt in this direction, via a series of numerical simulations of a swimmer in stratified waters, was carried out by Doostmohammadi *et al.* [30]. The results show that stratification has potential benefits, as it may render a microorganism less prone to be detected by predators, but on the flip side it demands more energy during locomotion. As a first approximation, the classic "two-mode squirmer" model is employed as a representative swimming microorganism [64]. This model consists of a spherical swimmer body with a prescribed tangential "slip" velocity that represents the effects of surface deformations due to flagella or cilia:

$$u_\theta = B_1 \sin\theta + \frac{B_2}{2} \sin 2\theta, \tag{7}$$

where θ is the inclination angle measured from the swimming direction. The parameters B_1 and B_2 determine the organism velocity and stress field around the organism, respectively. The sign of the ratio of $\beta = B_2/B_1$ distinguishes puller (generating thrust in front of the body) and pusher (generating thrust behind) swimmers with $\beta > 0$ for pullers (e.g., algal cells) and $\beta < 0$ for pushers (e.g., bacteria).

The results show that the stratification has major consequences on the motility of organisms and causes a dramatic reduction in their speed up to ∼50%, when compared to a homogeneous fluid [30]; see Fig. 6(b). There are two mechanisms responsible for reduced motility (alternatively, enhanced energetic needs): (i) viscous "trapping" of lower-density fluid from upper layers, resulting in the formation of a "shell" of lighter fluid around the organism [where the negative buoyancy of this fluid shell reduces the speed of the organism; Fig. 6(b)] and (ii) the "tail" of perturbed isopycnals in the organism's wake, which induces upward moving flows due to the tendency of isopycnals to restore to the unperturbed configuration.

The significant reduction in motility implies that the "flow signature" of organisms can be markedly altered by stratification. This is because of the suppression of vertical fluid flow—and thus reduced fluid disturbance in the ambient—as discussed in Sec. II A. It is quantified by calculating the volume wherein a fluid disturbance exceeds a threshold, i.e., a detection volume. Calculations show that the flow signature in a stratified fluid can be less than half of that in a homogeneous fluid; i.e., detection volumes can be ∼60% smaller. A direct consequence of low detection volumes is a possible safety offered against predators, due to reduced mechanosensing. Moreover, measurements of the energy expenditure by the microswimmers show a significant increase of up to 300% and 500%

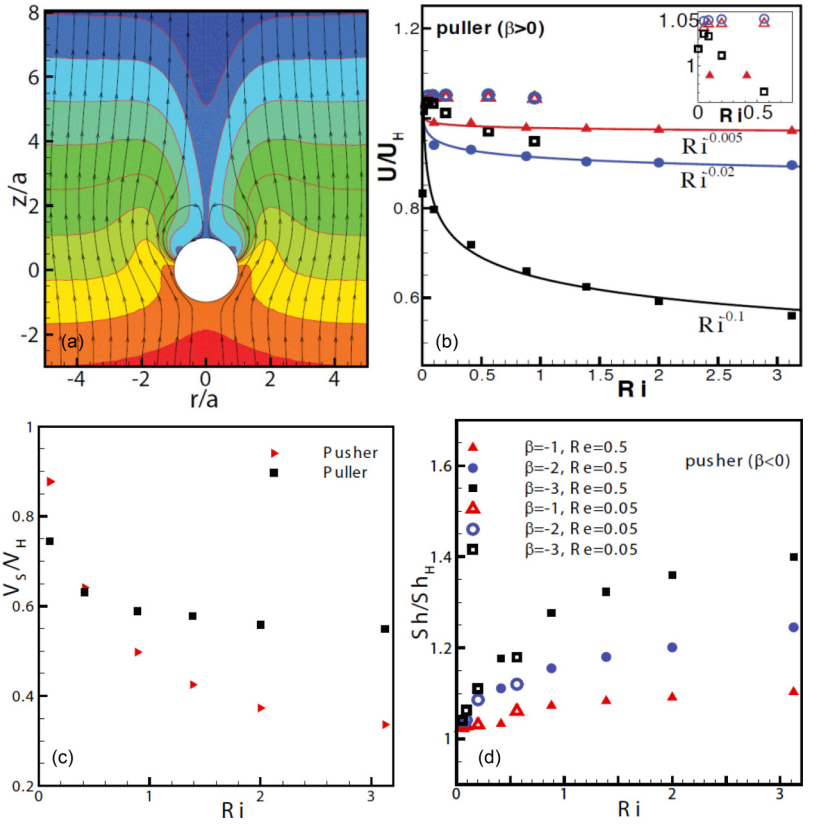

FIG. 6. Motility of microorganisms is affected by density stratification. (a) Stratification impact on the velocity field generated by squirmers. The color map shows normalized density. Black lines with arrows represent streamlines. Note that the squirmer is swimming in the downward $(-z)$ direction. (b) The speed of an organism in a stratified fluid, U, normalized by the speed in a homogeneous fluid, U_H, as a function of the Richardson number $\mathrm{Ri} = \mathrm{Re}/\mathrm{Fr}^2$ (higher Ri corresponds to stronger stratification). (c) Stratification leads to a significant reduction of the detection volume compared to a homogeneous fluid. (d) Stratification increases nutrient uptake compared to the homogeneous fluid. The nutrient uptake is quantified by the Sherwood number $\mathrm{Sh} = -\int \mathbf{n} \cdot \nabla C \, dS/(4\pi a C_\infty)$, measuring the ratio of the nutrient flux at the swimmer surface to the nutrient uptake by the diffusion alone. (Reprinted from [30] with the permission of the National Academy of Sciences.)

for pullers and pushers, respectively. This is because, in addition to working against hydrodynamic resistance, the organism also consumes energy as it mixes the ambient fluid, i.e., homogenizes the ambient density gradients. It is noteworthy that the disparity in the energy expenditure between pullers and pushers cannot be captured by the semianalytic point-force singularity method, discussed in Sec. II A, and this highlights the necessity of full numerical simulations. In addition, the results show that nutrient uptake of the organism can be largely affected by stratification. The nutrient concentration, C, is computed by solving the following conservation equation:

$$\frac{\partial C}{\partial t} + \mathbf{u} \cdot \nabla C = \kappa_N \nabla^2 C, \tag{8}$$

where κ_N is the nutrient diffusion coefficient. The effect of stratification is quantified by comparing the Sherwood number—representing the ratio of the total nutrient uptake to the nutrient uptake by diffusion alone—for stratified and homogeneous fluids. It is seen that for the parameter values considered, and at a fixed swimming speed, stratification leads to thinner concentration boundary

layers around a swimmer as compared to a homogeneous fluid, for both a pusher and a puller, implying enhanced diffusion of nutrients into the swimmer body. As a result, the Sh for a stratified system is larger than Sh_H for a homogeneous system, or $\mathrm{Sh}/\mathrm{Sh}_H > 1$ [see Fig. 6(d)]. But a higher Sh does not translate to more efficient foraging, because of the increased energetic expenditure discussed earlier. In other words, the "foraging efficiency" ($\eta_{\mathrm{for}} \equiv \mathrm{Sh}/P$, where P is the energy expended by the swimmer) for a stratified fluid is *always* less than that for a homogeneous fluid ($\eta_{\mathrm{for},H} \equiv \mathrm{Sh}_H/P_H$) and the ratio $\eta_{\mathrm{for}}/\eta_{\mathrm{for},H}$ continues to reduce for greater stratifications. These results are a reflection of the notable effects that stratification has on the livelihood of marine organisms. In conclusion, we reiterate that residing at pycnoclines leads to many fundamental changes in an organism's biophysical dynamics, the major ones being a reduction in the cell motility, as well as in the risk of their predation.

B. The role of stratification on bioconvection plumes of a suspension of gyrotactic algal cells

In this section, we discuss that not only does density stratification affect organisms individually, but that it also does so collectively, by hindering bioconvection and effecting aggregation. Bioconvection plumes emerge as groups of bottom-heavy microorganisms swim against gravity, following an external stimuli such as light or oxygen. This leads to an overturning instability *à la* Rayleigh-Bénard, as a heavier layer of swimmers over a lighter fluid creates a "top-heavy" situation (an unstable density gradient) [65]. Such bioconvection plumes have been observed in bacterial, flagellate, plankton, ciliate cultures, and algal cells [66]. We first focus on a particular form of bioconvection, which occurs for bottom-heavy algal cells, and is termed gyrotaxis. In gyrotaxis, an interplay between the viscous (due to fluid flow) and gravitational (due to bottom heaviness) torques acting on the cell body determines the swimming direction of the cell [67,68]. Towards this, we study the impact of density gradients—caused by heterogeneities in cell and salt concentration (or temperature distribution) combined—on bioconvection. We note that the stratification can be induced either by temperature or by salinity gradients. We emphasize here that since gyrotaxis-induced stratification is affected or controlled by cellular motility, gyrotactic bioconvection behaves differently as compared to the phenomenon of double diffusion (where the scalars being transported are "passive tracers" as opposed to "active swimmers") [69,70].

1. Continuum numerical approach

Karimi and Ardekani used coarse-grained three-dimensional computational modeling to investigate the dynamics of an algal suspension in a stratified fluid [56]. At the coarse-grained level, the cell concentration [number density, denoted by $n(\mathbf{x},t)$] is assumed to be continuous, with the condition $nv \ll 1$, where v is the average volume of a single algal cell. The ambient fluid velocity $\mathbf{u}$ is governed by the continuity and Navier-Stokes equations under the Boussinesq approximation:

$$\frac{\partial \mathbf{u}}{\partial t} + \mathbf{u}\cdot\nabla\mathbf{u} = -\nabla p_e - \mathrm{Sc}(Rn + \mathrm{Le}R_s T)\hat{\mathbf{z}} + \mathrm{Sc}\nabla^2\mathbf{u}, \quad \nabla\cdot\mathbf{u} = 0, \tag{9}$$

$$\frac{\partial n}{\partial t} + \mathbf{u}\cdot\nabla n = -\nabla\cdot(nV_c\mathbf{p}) + \nabla^2 n, \tag{10}$$

$$\frac{\partial T}{\partial t} + \mathbf{u}\cdot\nabla T = \mathrm{Le}\nabla^2 T, \tag{11}$$

where the dimensionless numbers are defined as follows: Schmidt number, $\mathrm{Sc} = \frac{\nu}{D}$; Lewis number, $\mathrm{Le} = \frac{\kappa}{D}$; dimensionless motility, $V_c = \frac{W_c L}{D}$; bioconvection Rayleigh number, $R = \frac{\bar{n} v \Delta\rho g L^3}{\rho_0 \nu D}$; and salinity/temperature Rayleigh number, $R_s = \frac{g\beta\Delta T L^3}{\nu\kappa}$, where $\Delta\rho$ is the excess density of the cells, $\bar{n}$ is the mean cell concentration, v is the average volume of a cell, W_c is the speed of the motile cells, $\mathbf{p}$ is the unit vector along the swimming direction, and the cell diffusion coefficient D is assumed to

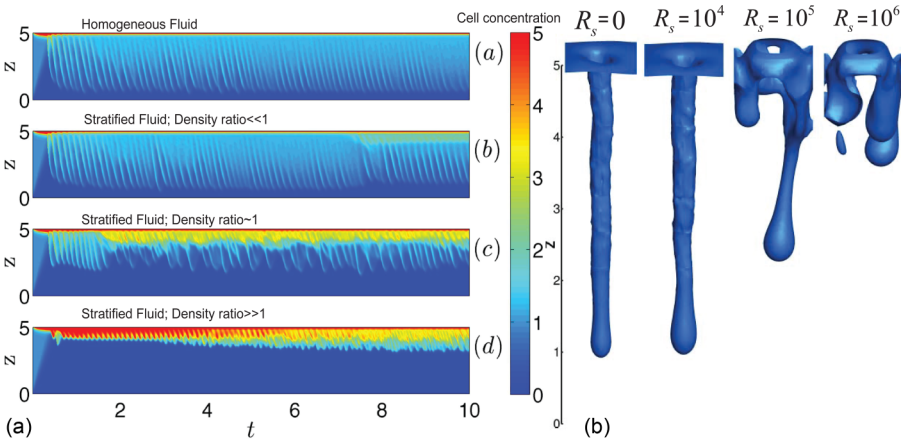

FIG. 7. (a) Space-time plots of the horizontal average of the cell concentration in a salt stratified fluid. (b) The isosurface of cell concentration for different values of density stratification. Density stratification hinders the bioconvection plumes and leads to the accumulation of algal cells at pycnoclines. (Reprinted from [56] with the permission of Cambridge University Press.)

be constant. The cell orientation $\mathbf{p}$ is governed by [71]

$$\dot{\mathbf{p}} = \frac{1}{2\tilde{B}}[\hat{\mathbf{z}} - (\hat{\mathbf{z}} \cdot \mathbf{p})\mathbf{p}] + \frac{1}{2}\boldsymbol{\omega} \times \mathbf{p} + \frac{r^2 - 1}{r^2 + 1}\mathbf{p} \cdot \mathbf{E} \cdot (\mathbf{I} - \mathbf{pp}), \tag{12}$$

where $\boldsymbol{\omega}$ is the local vorticity field, $\tilde{B} = 4\pi\mu a^3/mgh$ is a time scale for gyrotactic reorientation with a and m denoting cell radius and mass, respectively, $\mathbf{E} = (\nabla\mathbf{u} + \nabla\mathbf{u}^T)/2$ is the rate of strain tensor, and r is the aspect ratio of the cells. The center of mass of the cell is offset by a distance h from the center of buoyancy. The dimensionless gyrotactic parameter BD/L^2 is introduced to represent the ratio of the reorientation time of the gyrotactic cell to the required time for diffusing across the length L. In deriving Eq. (12), inertial effects are neglected and the balance between the torques induced by gyrotactic effects and viscous effects is incorporated [71].

The space-time representations of cell dynamics are illustrated in Fig. 7(a), and the isosurfaces of n for different levels of stratification can be seen in Fig. 7(b). When R_s is small, the negative buoyancy due to stratification is dominated by the viscous forces, and thus the plume dynamics is similar to the case of a homogenous fluid ($R_s = 0$). At higher R_s, stronger buoyancy suppresses downwelling of the algal cells—and concomitantly, bioconvection—leading to the cell accumulation at the top (free) surface. Karimi and Ardekani [56] noted that this transition in the dynamical behavior of the system is best represented by the "buoyancy ratio" $R_\rho = \mathrm{Le}R_s/R = \rho_0\beta\Delta T/(\bar{n}v\Delta\rho)$, characterizing the relative effects of buoyant forces due temperature or salinity, and cell concentration. Numerical simulations for different values of Rayleigh number, Lewis number [corresponding to both temperature (Le $>$ 1) and salinity stratification (Le $<$ 1)], Schmidt number, and motility (representing various planktonic species) were performed for both sharp and linearly stratified fluid domains. Finally, Karimi and Ardekani [56] also performed a linear stability analysis, providing the threshold for the onset of gyrotactic bioconvection instability in the presence of stratification.

2. Accumulation of algal cells in stratified fluids: Experimental approach

A biflagellate gyrotactic organism, *Heterosigma akashiwo*, forms toxic algal blooms in temperate waters [72]. The flagellum along the direction $\mathbf{p}$ is responsible for generating a propulsion velocity in that direction. A second flagellum, along $\mathbf{n}$, generates an intrinsic torque which creates the helical motion of the cell (see Fig. 8). It has been shown that changes in salinity of the environment trigger

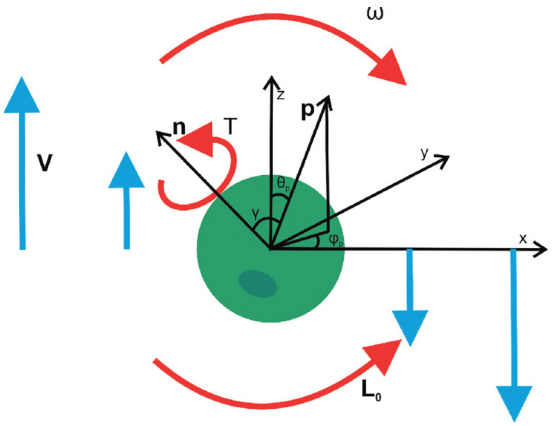

FIG. 8. A schematic of an algal cell like *Heterosigma akashiwo*, that utilizes two flagella—directed along the unit vectors **p** and **n**—for swimming. (Reprinted from [73] with the permission of AIP.)

the formation of *Heterosigma* blooms, for instance after a freshwater runoff from rivers or a sudden rain storm [12]. Despite this, the role of stratification on the cell distribution is poorly understood, with only a few experiments focusing solely on collective cellular motion in stratified domains.

Hershberger *et al.* demonstrated that *Heterosigma akashiwo* cells aggregated below the interface (halocline) between a high salinity fluid (at the bottom) and a low salinity fluid (at the top) [74]. They did not observe any such aggregation in cases where an interface was absent, i.e., when the fluid in the test tubes was either salt free (freshwater), or had a constant salinity. This latter observation might have been due to bioconvective mixing, because a subsequent study by Bearon *et al.* did report the occurrence of surface aggregation, even in unstratified fluids, within ∼2 h after the initial injection of the algal cells into the water column [75]. This aggregation soon led to an overturning instability leading to the formation of bioconvection plumes, and subsequent fluid mixing. The objective of Bearon *et al.*'s study was to analyze the effect of a sharp salinity stratification on the swimming behavior of *Heterosigma* cells [75]. The sharp stratification was realized by overlaying a heavier fluid column with a lighter one, with the strength of stratification dictated by the corresponding salinities. They estimated the cell concentration by observing and recording the number of two-dimensional trajectories of up-swimming cells in the water column, with the main conclusion being that the cells' swimming behavior depended on the strength of the "salinity jump." The behavior did not change appreciably when the jump was from a 28% saline solution to a 16% saline solution. But when the jump was from a 28% saline solution to freshwater (0% saline), strong aggregation (one order of magnitude difference between top and bottom algal concentration) was observed, with the cells stopping altogether at the halocline. They attributed this behavior to an increase in the cell diameter in regions of low salinity—due to osmosis of the "fresher" water into the cell bodies—leading to increased drag, and hence reduced velocity. Based on this hypothesis, their calculations of the Stokes drag agreed well with the experimental observations. In a later study, Bearon and Grünbaum studied the formation of bioconvection patterns of upswimming *Heterosigma* in stratified fluids [76]. They carried out experiments (i) in a weakly stratified fluid and (ii) in a sharply stratified one (like the study of Hershberger *et al.*). In case i, they observed the classic overturning instability and the formation of bottom-standing bioconvection plumes. In case ii, initially, in the absence of stratification, the algal suspension was well mixed due to the aforementioned bioconvection. But the addition of a low salinity fluid onto the upper surface resulted in a rapid (on the order of minutes) upswimming of cells, followed by visible aggregation below the air-water interface.

In order to estimate the cell concentration as a function of position in HABs, it is important to measure the spatial heterogeneity in the cell population. The lack of quantitative experimental studies on HABs motivated us to estimate the concentration of *Heterosigma* aggregates in a salt stratified

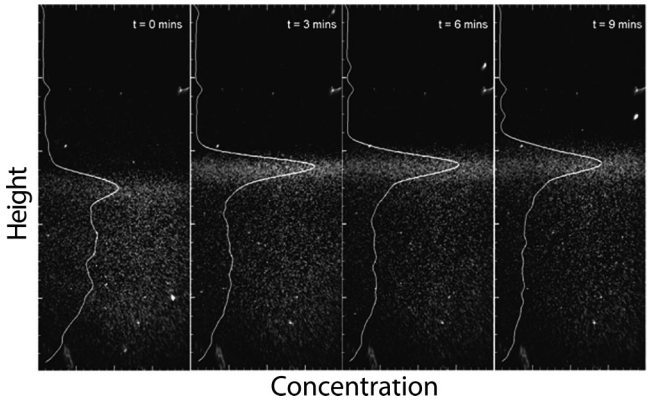

FIG. 9. Aggregation of *Heterosigma akashiwo* at the halocline. Conditions are cell density 2.5×10^6 in $f/2$ media ($1.024\ \mathrm{g/cm^3}$).

environment, using dark field image analysis. *Heterosigma akashiwo* (strain CCMP452, Bigelow Laboratory) was cultured in $f/2$ medium and synchronized via a 12:12 light:dark (LD) photoperiod at 25 °C. Exponentially growing cells at a concentration of 2.5×10^6 cells/cm^3 were visualized in a cuvette cell. A sharp stratified environment was created by slowly adding distilled water on top of algal suspension. The relative density of the medium and distilled water was measured by a density meter (Densito 30PX, Mettler Toledo). The dark field illumination was provided with a circular light-emitting diode array (3.6 cm diameter, 655 nm emission; Advanced Illumination), to which the algal cells are insensitive; i.e., the possibility of phototaxis is prevented. The cells were observed in a dark and unstratified condition first, to confirm the upward swimming. All images were captured by a high speed camera (Vision Research M340, Phantom) at 60 frames/s with a 24× objective. The results clearly show the accumulation of cells at the density interface (Fig. 9).

The behavior of organisms (dinoflagellates and *Heterosigma akashiwo*) in stratified fluids encompasses many other nontrivial aspects that are unexplored so far. The phenomenon as a whole is governed by interactions between inertial, viscous, and buoyancy forces, but there are a number of additional underlying complexities that must be unraveled. The most important one is turbulence, which is ubiquitous in marine environments. There are a number of organisms in the oceans that have characteristic dimensions larger than the Kolmogorov length scale; consequently the effect of turbulent flow regimes on the motion of these organisms should be considered. It is expected that the velocity fluctuations in space and time will be affected by background density gradients as well as the swimming motion, and care must be taken to account for this. The density gradient will have a stabilizing effect, while the swimming motion coupled with turbulent velocity fluctuations will tend to enhance the randomness, thus giving rise to a unique confluence.

C. Biogenic mixing and the role of stratification and turbulence

The energy input of biological activities in the oceans has been claimed to be of the same order as major storms [77]. It is argued that marine organisms whose swimming Reynolds numbers range from $O(1)$ to $O(1000)$ contribute significantly in global ocean mixing [78–83] through biogenic turbulence or drift mechanisms. However, there are contradictory arguments dismissing the idea by attributing a low mixing efficiency to biogenic mixing and a small drift volume due to restoration of deflected density levels [84,85]. The problem is yet to be resolved since the comprehensive knowledge of fluid-organism interaction is not available to fully understand the relevant mechanisms involved in biogenic mixing. Moreover, the fluid dynamics of the ocean is largely affected by density stratification, and an accurate quantification of biogenic mixing requires a consistent incorporation

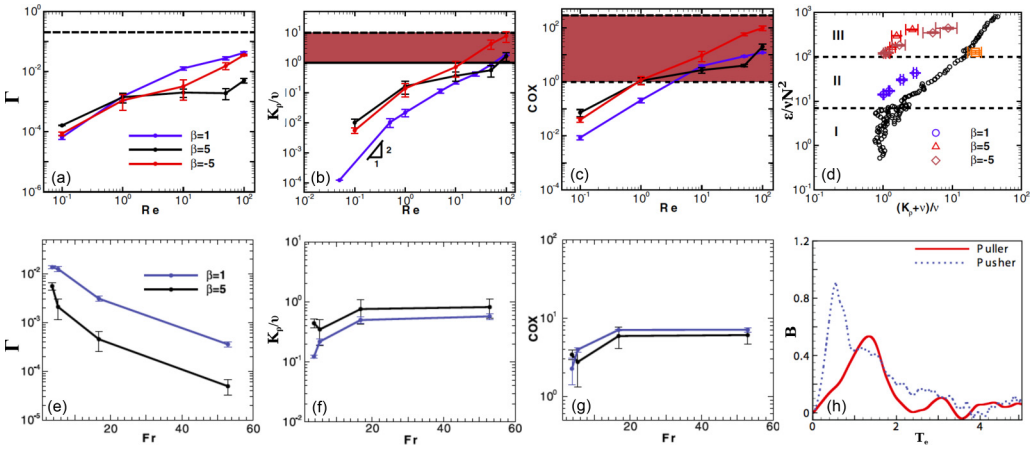

FIG. 10. The effect of the Reynolds number on (a) the mixing efficiency Γ, (b) the diapycnal eddy diffusivity κ_ρ, and (c) the Cox number. (d) The comparison of the turbulent activity parameter $\epsilon/\nu N^2$, between the swimmer-induced mixing and the shear-driven turbulence (black circles). The impact of density stratification on (e) mixing efficiency, (f) diapycnal eddy diffusivity, and (g) the Cox number. (h) The temporal evolution of the active biomixing number for pushers and pullers, where $T_e = t/\tau_0$ is the normalized time scale and τ_0 is the initial eddy turnover time of the turbulence. (Reprinted from [35] with the permission of Nature Publishing Group.)

of these effects. Studies on suspensions of particles have shown that particle assembly can enhance mixing in temperature stratified fluids through hydrodynamics of the particle motion coupled with the tendency of the particles to themselves act as heat carriers [86]. However, whether this enhancement is large enough to contribute to ocean mixing is subject to further investigation. Recently, Wang and Ardekani [35] have tackled the problem of biogenic mixing by conducting direct simulations of suspensions of squirmers, taking into account the effects of viscous and inertial forces, hydrodynamic interactions between the swimmers, density stratification, and also background turbulence in the fluid. The results are presented for a range of Reynolds numbers Re $\sim O(1-100)$ that is relevant to the zooplankton that are abundant in the ocean.

The following three measures were computed to quantify the impact of the swimming organisms on biogenic mixing: (1) the efficiency of biogenic mixing Γ, which is the ratio of the rate of energy removal by buoyancy forces to the total kinetic energy in the fluid domain, (2) the diapycnal eddy diffusivity K_ρ, which characterizes the mixing induced by the vertical transport of the organisms, and (3) the Cox number COX, which quantifies the variation in the temperature gradients in the fluid and is an indicator of the temperature microstructure.

The impact of inertia on the biogenic mixing is quantified by calculating the variation of Γ, K_ρ, and COX as a function of the Reynolds number [see Figs. 10(a)–10(c)]. As evident from Fig. 10, larger inertia of the swimming organisms leads to enhanced mixing by increasing the mixing efficiency, the extent of vertical transport, and the average temperature variations in the domain. It was further shown by Wang and Ardekani that the mixing is more pronounced for vertically swimming squirmers than for the horizontally (perpendicular to gravity) swimming ones, with K_ρ and COX being two orders of magnitude larger [35]. Moreover, in order to characterize the vertical transport by biogenic mixing with respect to the pseudoturbulence effects that are generated by the fluctuations in the organisms' velocities, the turbulent activity parameter $R_a = \epsilon/\nu N^2$ is plotted as a function of normalized diapycnal eddy diffusivity $(K_\rho + \nu/)\nu$ [see Fig. 10(d)]. Here, $\epsilon = 2\nu\mathbf{E} : \mathbf{E}$ is the viscous dissipation defined based on the strain rate tensor $\mathbf{E}$ for fluctuating velocities. Small ($R_a < 7$), moderate ($7 < R_a < 100$), and large ($R_a > 100$) activity numbers correspond to decaying, stationary, and growing turbulence in stratified fluids, respectively. The results show that mixing

predominantly occurs at large activity numbers, indicating that the strong eddy diffusivity generated by swimmers corresponds to larger energy dissipation as compared to turbulent mixing. It should be noted that the mixing efficiency of swimmers is found to be much smaller than the mixing efficiency measured in the ocean for turbulent mixing. Wang and Ardekani [35] also considered the impact of density stratification on the mixing induced by organisms [see Figs. 10(e)–10(g)]. As the strength of the stratification is decreased (i.e., as the Froude number is increased), the mixing efficiency is significantly reduced, while the vertical flux and temperature microstructure reach steady values and become independent of stratification for Fr ~ 20. This value of the Froude number corresponds to the stratification length scale being larger than the organism size.

In natural waters, the background turbulence in the fluid can interfere with stratification effects. The strongest velocity gradients due to turbulence occur at a length scale of (10–50)L_K, where L_K is the Kolmogorov scale, $L_K = (\nu^3/\epsilon)^{1/4}$, and ϵ is the turbulent dissipation rate [87]. For $\epsilon = 1 \times 10^{-8}$/W/kg [88–90], this length scale is 32–158 mm. The scalar gradient length scales are smaller than the velocity gradient length scales by a factor of $\mathrm{Pr}^{1/2}$, leading to the length scales of 1–6 mm (10–60 mm), at which turbulence can impact velocity fields of motile organisms in stratified fluids caused by salt (temperature) gradients. The weaker turbulence observed in inlets [82], lakes, and reservoirs [91] increases these length scales. The intermittent nature of the turbulence [87] is expected to occasionally destroy the flow field of millimeter-sized organisms in weakly turbulent flows. On the other hand, under strong turbulent flows, the flow field is significantly modified and turbulence can affect the transport of particles and organisms.

In order to study the hydrodynamic interactions between turbulence and the disturbances induced by the swimmers, a statistically steady stratified turbulence is numerically generated and treated as the initial background flow. For generating the statistically steady stratified turbulence, Eqs. (1) to (3) are solved. A direct forcing term, $\boldsymbol{f} = \rho_0\epsilon/\overline{\boldsymbol{u}\cdot\boldsymbol{u}}$, is added to the momentum equation to achieve statistically steady state stratified turbulence [92,93]. The initial temperature field varies linearly with depth and the initial velocity field is generated using the open source code NTMIX-3D [94]. The initial velocity profile has the following energy spectrum $E(\boldsymbol{k})$ (see [95]):

$$E(\boldsymbol{k}) = A\left(\frac{\boldsymbol{k}}{\boldsymbol{k}_e}\right)^4 \exp\left(-2\left(\frac{\boldsymbol{k}}{\boldsymbol{k}_e}\right)^2\right), \tag{13}$$

where $\boldsymbol{k}$ is the wave number, $\boldsymbol{k}_e$ is the most energetic wave number, and $A = (16u_{\mathrm{rms}}^2/\boldsymbol{k}_e^2)\sqrt{2/\pi}$ with u_{rms} being the root-mean-square value of the fluid velocity. The statistically stationary state for the turbulence is reached, as both u_{rms}^2 and ϵ reach their quasisteady values. The grid size is chosen such that the Kolmogorov scale is well resolved in the simulations. One of the main advantages of the DNS of biogenic mixing in stratified turbulence is that it allows for dissecting the effect of swimming organisms on mixing from the impact of the background turbulence. To achieve this, a "biomixing active parameter" $B = K_{\rho,\mathrm{bio}}/K_{\rho,\mathrm{turb}}$ is defined as the ratio of the diapycnal eddy diffusivity due to biogenic mixing, $K_{\rho,\mathrm{bio}}$, to its counterpart due to turbulent mixing, $K_{\rho,\mathrm{turb}}$. The temporal evolution of biomixing active parameter reveals the existence of two distinct regimes for both pushers and pullers [see Fig. 10(h)]. During the early stages of mixing, hydrodynamic interactions between the fluctuations induced by swimmers and by the background turbulence generate a large biomixing activity number ($B > 0.2$). Interestingly, during the first stage, the turbulence-induced mixing is amplified more by the pushers than by the pullers. This is due to the difference in the nature of hydrodynamic interactions between pushers and pullers, which leads to rectilinear trajectories of the former as opposed to helical trajectories of the latter [41]. Taken together, these results show that although swimming strategy is important at local swimming scales in producing efficient biogenic mixing and enhancing the vertical transport, it does not play a significant role at global scales.

V. CONCLUDING REMARKS

The presence of density gradients in the water column (density stratification) is an important factor in governing the hydrodynamics of settling and swimming in environmental flows, irrespective of

whether it is a single particle settling in the ocean or an assembly of motile phytoplankton forming large-scale blooms. In an aqueous medium, the density stratification can be caused by temperature or salinity variations and manifests in the form of a sharp density interface or a continuous density gradient (e.g., linear stratification). There is now a growing evidence on the correlation between local hot spots engendered by density stratification and accumulation of particles and/or increased activity of organisms in the vicinity of these hot spots. Here, we provided an overview of recent works on settling of particles and swimming of organisms in stratified fluids. We presented a comprehensive computational study of settling dynamics in stratified fluids, from rigid particles and deformable drops to self-propelled organisms. In addition to individual particles and organisms, our studies shed light on the hydrodynamics of particle suspensions and on organism blooms.

We began by considering a linearized set of the governing equations and using point-force singularities to account for the presence of a single particle or a force-free swimmer. This allowed a tractable semianalytical approach to tackle the problem of settling and swimming in stratified fluids, providing qualitative predictions of the impact of density stratification on the vertical motion of particles and microswimmers. Next, we complemented the semianalytical approach by simulations of full nonlinear equations accounting for the interactions between a stratified medium, and rigid, deformable, and self-propelled particles. The numerical simulations, for a single spherical particle settling through sharp and linear stratifications, provided a quantitative understanding of different regimes of settling dynamics and the emergence of vortex structures and lee waves around the particle. We then studied the dynamics of a pair of particles in a stratified fluid, exploring the impact of the fluid density variations on the interaction between the two particles as a building block to study particle suspension in stratified fluids. In the end, we introduced self-propulsion as an extra complexity to explore the effect of density stratification on the vertical migration of a microswimmer and on the mixing induced by a suspension of small organisms. In addition to DNS of multiple swimmers, we developed a continuum approach to characterize the bioconvection patterns of swimmer suspensions in stratified fluids and finally summarized some of the relevant experimental studies in the realm of bioconvection in stratified media.

A noteworthy aspect of the present review is that certain characteristics of the motion of multiple particles or drops can be inferred by a careful examination of the motion of a single particle or drop, and of the interactions between a pair of particles or drops. In fact, the idea of suppression of vertical motion, conveyed in Sec. II A, is a fundamental mechanism underpinning the major results discussed in the subsequent sections: from the slower terminal velocity of a single settling particle, to the reduced vertical velocity fluctuations in a suspension of settling particles. It is also seen that stratification affects a single drop and a swarm of drops in a similar manner, i.e., by reducing the average rise velocity in both cases. However, it must be noted that this reduction is much more significant for the swarm, particularly at higher stratifications. The similarity between multiple particle or drop systems and a pair of particles or drops was also highlighted in Sec. III B, where we saw peaks in the values of the pairwise probability distribution function $[G(\theta)]$ for a suspension of settling particles, for $\theta = 0,\ \pi/2,\ \pi$. These peaks were explained based on the results obtained for the motion of a pair of particles: (i) enhanced attraction in side-by-side configurations explained the enhanced peaks at $\theta = \pi/2$, and (ii) absence of a tumbling regime in tandem settling (at high stratifications) explained the peaks at $\theta = 0,\ \pi$. Finally, the emerging coherence between the theory of suspensions and that of pairwise interactions leads us to postulate that the even more involved phenomena seen in suspensions of microorganisms in stratified fluids can be explained if the pairwise interactions of said microorganisms are investigated under identical conditions of fluid flow [41] and stratification.

Our studies have shown that by suppressing the vertical motion of particles, drops, and organisms, density stratification plays a key role in the formation of particle, drop, and organism clusters. Moreover, the bioconvection plumes of algal cells are shown to be markedly affected by temperature or salinity gradients, indicating a potential mechanism of affecting algal bloom formation. In addition, the ecological traits of a single organism—e.g., its nutrient uptake, detectability, and energy expenditure—are shown to experience dramatic changes due to the modification of its flow

signature in a linearly stratified fluid. It is further shown that not only is the swimming dynamics affected by stratification in the fluid, but that collective swimming of organisms can also lead to prominent changes in transport properties such as mixing of the isopycnals. This study provided an intricate coupling between organism behavior and stratification. The presence of background turbulence adds to this complexity by contributing to the mixing of the fluid. The numerical approach presented in this paper provides a tractable means for dissecting impacts of these interconnected mechanisms by accounting for inertial and viscous forces, stratification, organism-induced mixing, and turbulence-induced mixing. It is found that at the local scale, the diapycnal eddy diffusivity due to interacting swimmers is comparable with the one from internal waves in the mid-ocean. However, this is a local effect and at the global oceanic level, swimming organisms are expected to have a small contribution to the overall ocean mixing.

ACKNOWLEDGMENTS

This research is supported by the National Science Foundation, Grants No. CBET-1066545 and No. CBET-1604423. We would thank Glareh Azadi, Tiago Rosa dos Reis, and Harris Hassan for their help in the experiment.

[1] M. Z. Jacobson, Aerosol scattering and absorption, in *Fundamentals of Atmospheric Modeling* (Cambridge University Press, Cambridge, UK, 1998).

[2] S. MacIntyre, A. L. Alldredge, and C. C. Gotschalk, Accumulation of marine snow at density discontinuities in the water column, Limnol. Oceanogr. **40**, 449 (1995).

[3] A. L. Alldredge and C. C. Gotschalk, Direct observations of the mass flocculation of diatom blooms: Characteristics, settling velocities and formation of diatom aggregates, Deep Sea Res. Part A **36**, 159 (1989).

[4] A. Capotondi, M. A. Alexander, N. A. Bond, E. N. Curchitser, and J. D. Scott, Enhanced upper ocean stratification with climate change in the CMIP3 models, J. Geophys. Res. **117**, C04031 (2012).

[5] J. E. Cloern, Temporal dynamics and ecological significance of salinity stratification in an estuary (South San Francisco Bay, USA), Oceanol. Acta **7**, 137 (1984).

[6] S. A. Henson, R. Sanders, E. Madsen, P. J. Morris, F. L. Moigne, and G. D. Quartly, A reduced estimate of the strength of the ocean's biological carbon pump, Geophys. Res. Lett. **38**, L04606 (2011).

[7] R. Stone, The invisible hand behind a vast carbon reservoir, Science **328**, 1476 (2010).

[8] B. S. Sherman, I. T. Webster, G. J. Jones, and R. L. Oliver, Transitions between *Auhcoseira* and *Anabaena* dominance in a turbid river weir pool, Limnol. Oceanogr. **43**, 1902 (1998).

[9] J. R. Geraci, J. Harwood, and V. J. Lounsbury, Marine mammal die-offs: Causes, investigations, and issues, in *Conservation and Management of Marine Mammals* (Smithsonian Institution Press, Washington, DC, 1999), pp. 367–395.

[10] J. Harwood, Mass die-offs, in *Encyclopedia of Marine Mammals* (Academic Press, San Diego, CA, 2002), pp. 724–726.

[11] P. Gentien, M. Lunven, M. Lehaître, and J. L. Duvent, In-situ depth profiling of particle sizes, Deep-Sea Res. Part I, **42**, 1297 (1995).

[12] F. J. R. Taylor and R. Haigh, The ecology of fish-killing blooms of the chloromonad flagellate *Heterosigma* in the Strait of Georgia and adjacent waters, *Toxic Phytoplankton Blooms in the Sea* (Elsevier, Amsterdam, 1993).

[13] M. J. Pennino, S. S. Kaushal, J. J. Beaulieu, P. M. Mayer, and C. P. Arango, Effects of urban stream burial on nitrogen uptake and ecosystem metabolism: Implications for watershed nitrogen and carbon fluxes, Biogeochemistry **121**, 247 (2014).

[14] K. G. Sellner, G. J. Doucette, and G. J. Kirkpatrick, Harmful algal blooms: Causes, impacts and detection, J. Ind. Microbiol. Biotech. **30**, 383 (2003).

[15] A. M. Ardekani and R. Stocker, Stratlets: Low Reynolds Number Point-Force Solutions in a Stratified Fluid, Phys. Rev. Lett. **105**, 084502 (2010).
[16] O. M. Phillips, On flows induced by diffusion in a stably stratified fluid, Deep Sea Res. **17**, 435 (1970).
[17] H. Hanazaki, A numerical study of three-dimensional stratified flow past a sphere, J. Fluid Mech. **192**, 393 (2000).
[18] M. D. Greenslade, Drag on a sphere moving horizontally in a stratified fluid, J. Fluid Mech. **418**, 339 (2000).
[19] J. C. R. Hunt and W. H. Snyder, Experiments on stably and neutrally stratified flow over a model three-dimensional hill, J. Fluid Mech. **96**, 671 (2006).
[20] R. C. Y. Koh, Viscous stratified flow towards a sink, J. Fluid Mech. **24**, 555 (1966).
[21] J. S. Turner, *Buoyancy Effects in Fluids* (Cambridge University Press, Cambridge, UK, 1973).
[22] A. N. Srdić-Mitrović, N. A. Mohamed, and H. J. S. Fernando, Gravitational settling of particles through density interfaces, J. Fluid Mech. **381**, 175 (1999).
[23] C. R. Torres, H. Hanazaki, J. Ochoa, J. Castillo, and M. Van Woert, Flow past a sphere moving vertically in a stratified diffusive fluid, J. Fluid Mech. **417**, 211 (2000).
[24] H. Hanazaki, K. Konishi, and T. Okamura, Schmidt-number effects on the flow past a sphere moving vertically in a stratified diffusive fluid, Phys. Fluids **21**, 026602 (2009).
[25] K. Y. Yick, C. R. Torres, T. Peacock, and R. Stocker, Enhanced drag of a sphere settling in a stratified fluid at small Reynolds numbers, J. Fluid Mech. **632**, 49 (2009).
[26] D. Stramski, A. Bricaud, and A. Morel, Modeling the inherent optical properties of the ocean based on the detailed composition of the planktonic community, Appl. Optics **40**, 2929 (2001).
[27] E. J. List, Laminar momentum jets in a stratified fluid, J. Fluid Mech. **45**, 561 (1971).
[28] N. Liron and J. R. Blake, Existence of viscous eddies near boundaries, J. Fluid Mech. **107**, 109 (1981).
[29] A. Doostmohammadi, S. Dabiri, and A. M. Ardekani, A numerical study of the dynamics of a particle settling at moderate Reynolds numbers in a linearly stratified fluid, J. Fluid Mech. **570**, 5 (2014).
[30] A. Doostmohammadi, R. Stocker, and A. M. Ardekani, Low-Reynolds-number swimming at pycnoclines, Proc. Natl. Acad. Sci. USA **109**, 3856 (2012).
[31] A. Doostmohammadi and A. M. Ardekani, Reorientation of elongated particles at density interfaces, Phys. Rev. E **90**, 033013 (2014).
[32] S. Bayareh, A. Doostmohammadi, and A. M. Ardekani, On the rising motion of a drop in stratified fluids, Phys. Fluids **25**, 103302 (2013).
[33] A. Doostmohammadi and A. M. Ardekani, Suspension of solid particles in a density stratified fluid, Phys. Fluids **27**, 023302 (2015).
[34] S. Dabiri, A. Doostmohammadi, S. Bayareh, and A. M. Ardekani, Numerical simulation of the buoyant rise of a suspension of drops in a linearly stratified fluid, Int. J. Multiphase Flows **69**, 8 (2015).
[35] S. Wang and A. M. Ardekani, Biogenic mixing induced by intermediate Reynolds number swimming at pycnoclines, Sci. Rep. **5**, 17448 (2015).
[36] A. M. Ardekani and R. H. Rangel, Numerical investigation of particle-particle and particle-wall collisions in a viscous fluid, J. Fluid Mech. **596**, 437 (2008).
[37] A. M. Ardekani, S. Dabiri, and R. H. Rangel, Collision of multi-particle and general shape objects in a viscous fluid, J. Comput. Phys. **227**, 10094 (2008).
[38] S. Dabiri and P. Bhuvankar, Scaling law for bubbles rising near vertical walls, Phys. Fluids **28**, 062101 (2016).
[39] R. Glowinski, T. W. Pan, T. I. Hesla, and D. D. Joseph, A distributed Lagrange multiplier fictitious domain method for particulate flows, Int. J. Multiphase Flow **25**, 755 (1999).
[40] G. Li and A. M. Ardekani, Hydrodynamic interaction of micro-swimmers near a wall, Phys. Rev. E **90**, 013010 (2014).
[41] G. Li, A. Ostace, and A. M. Ardekani, Hydrodynamic interaction of swimming organisms in an inertial regime, Phys. Rev. E **94**, 053104 (2016).
[42] G. Li and A. M. Ardekani, Collective Motion of Microorganisms in a Viscoelastic Fluid, Phys. Rev. Lett. **117**, 118001 (2016).
[43] G. Li and A. M. Ardekani, Undulatory swimming in non-Newtonian fluids, J. Fluid Mech. **784**, R4 (2015).

[44] R. Camassa, C. Falcon, J. Lin, R. M. McLughlin, and R. Parker, Prolonged residence times for particles settling through stratified miscible fluids in the Stokes regime, Phys. Fluids **21**, 031702 (2009).
[45] R. Camassa, C. Falcon, J. Lin, R. M. McLaughlin, and N. Mykins, A first-principle predictive theory for a sphere falling through sharply stratified fluid at low Reynolds number, J. Fluid Mech. **664**, 436 (2010).
[46] F. Blanchette and A. M. Shapiro, Drops settling in sharp stratification with and without Marangoni effects, Phys. Fluids **24**, 042104 (2012).
[47] S. Okino, S. Akiyama, and H. Hanazaki, Velocity distribution around a sphere descending in a linearly stratified fluid, J. Fluid Mech. **826**, 759 (2017).
[48] L. Díaz-Damacillo, A. Ruiz-Angulo, and R. Zenit, Drift by air bubbles crossing an interface of a stratified medium at moderate Reynolds number, Int. J. Multiphase Flow **85**, 258 (2016).
[49] I. Morris, *The Physiological Ecology of Phytoplankton* (University of California Press, Berkeley, CA, 1980).
[50] W. R. Clavano, E. Boss, and L. Karp-Boss, Inherent optical properties of non-spherical marine-like particles—from theory to observation, Oceanogr. Mar. Biol. **45**, 1 (2007).
[51] D. J. Jeffrey and Y. Onishi, Calculation of the resistance and mobility functions for two unequal rigid spheres in low-Reynolds-number flow, J. Fluid Mech. **139**, 261 (1984).
[52] R. G. Cox, The motion of long slender bodies in a viscous fluid. Part 2. Shear flow, J. Fluid Mech. **45**, 625 (1971).
[53] F. Fonseca and H. J. Herrmann, Simulation of the sedimentation of a falling oblate ellipsoid, Physica A **345**, 341 (2005).
[54] T. Pan, R. Glowinski, and G. P. Galdi, Direct simulation of the motion of a settling ellipsoid in Newtonian fluid, J. Comput. Appl. Math. **149**, 71 (2002).
[55] L. G. Leal, Particle motions in a viscous fluid, Annu. Rev. Fluid Mech. **12**, 435 (1980).
[56] A. Karimi and A. M. Ardekani, Gyrotactic bioconvection at pycnoclines, J. Fluid Mech. **773**, 245 (2013).
[57] A. Doostmohammadi and A. M. Ardekani, Interaction between a pair of particles settling in a stratified fluid, Phys. Rev. E **88**, 023029 (2013).
[58] M. Bayareh, S. Dabiri, and A. M. Ardekani, Interaction between two drops ascending in a linearly stratified fluid, Eur. J. Mech. B Fluids **60**, 127 (2016).
[59] É. Guazzelli and J. Hinch, Fluctuations and instability in sedimentation, Annu. Rev. Fluid Mech. **43**, 97 (2011).
[60] C. B. Field, Primary production of the biosphere: Integrating terrestrial and oceanic components, Science **281**, 237 (1998).
[61] J. S. Guasto, R. Rusconi, and R. Stocker, Fluid mechanics of planktonic microorganisms, Annu. Rev. Fluid Mech. **44**, 373 (2012).
[62] R. Stocker and J. R. Seymour, Ecology and physics of bacterial chemotaxis in the ocean, Microbiol. Mol. Biol. Rev. **76**, 792 (2012).
[63] M. T. Madigan, J. M. Martinko, K. S. Bender, D. H. Buckley, and D. A. Stahl, *Brock Biology of Microorganisms*, 14th ed. (Pearson, New York, 2014).
[64] J. Lighthill, Flagellar hydrodynamics, SIAM Rev. **18**, 161 (1976).
[65] N. A. Hill and T. J. Pedley, Bioconvection, Fluid Dyn. Res. **37**, 1 (2005).
[66] M. S. Plesset and H. Winet, Bioconvection patterns in swimming microorganism cultures as an example of Rayleigh-Taylor instability, Nature (London) **248**, 441 (1974).
[67] J. O. Kessler, Hydrodynamic focusing of motile algal cells, Nature (London) **313**, 218 (1985).
[68] T. J. Pedley and J. O. Kessler, Hydrodynamic phenomena in suspensions of swimming microorganisms, Annu. Rev. Fluid Mech. **24**, 313 (1992).
[69] J. S. Turner, *Buoyancy Effects in Fluids* (Cambridge University Press, Cambridge, UK, 1973).
[70] H. E. Huppert and J. S. Turner, Double-diffusive convection, J. Fluid Mech. **106**, 299 (1981).
[71] T. J. Pedley and J. O. Kessler, The orientation of spheroidal microorganisms swimming in a flow field, Proc. R. Soc. B Biol. Sci. **231**, 47 (1987).
[72] T. J. Smayda, Ecophysiology and bloom dynamics of *Heterosigma akashiwo* (Raphidophyceae), NATO ASI Ser. Ser. G **41**, 113 (1998).

[73] M. S. Alqarni and R. N. Bearon, Transport of helical gyrotactic swimmers in channels, Phys. Fluids **28**, 071904 (2016).
[74] P. K. Hershberger, J. E. Rensel, A. L. Matter, and F. B. Taub, Vertical distribution of the chloromonad flagellate *Heterosigma carterae* in columns: Implications for bloom development, Can. J. Fish. Aquat. Sci. **54**, 2228 (1997).
[75] R. N. Bearon and D. Grünbaum, Bioconvection in a stratified environment: Experiments and theory, Phys. Fluids **18**, 127102 (2006).
[76] R. N. Bearon, D. Grunbaum, and R. A. Cattolico, Effects of salinity structure on swimming behavior and harmful algal bloom formation in *Heterosigma akashiwo*, a toxic raphidophyte, Mar. Ecol. Prog. Ser. **306**, 153 (2006).
[77] B. MacKenzie and W. Laggett, Wind-based models for estimating the dissipation rates of turbulent kinetic energy in aquatic environments: Empirical comparison, Mar. Ecol. Prog. Ser. **94**, 207 (2010).
[78] W. H. Munk, Abyssal recipes, Deep Sea Res. **13**, 707 (1996).
[79] R. L. Iverson, D. P. Novacek, L. C. Laurent, W. K. Dewar, R. J. Bingham, and P. H. Wiebe, Does the marine biosphere mix the ocean? J. Mar. Res. **64**, 541 (2006).
[80] K. Katija and J. O. Dabiri, A viscosity-enhanced mechanism for biogenic ocean mixing, Nature (London) **460**, 624 (2009).
[81] K. Katija, Review: Biogenic inputs to ocean mixing, J. Exp. Biol. **215**, 1040 (2012).
[82] E. Kunze, J. F. Dower, R. Dewey, and E. A. D'Asaro, Mixing it up with krill, Science **318**, 1239 (2006).
[83] K. Katija, Morphology alters fluid transport and the ability of organisms to mix oceanic waters, Integr. Comp. Biol. **55**, 698 (2015).
[84] G. Subramanian, Viscosity-enhanced bio-mixing of the oceans, Curr. Sci. **98**, 1103 (2010).
[85] A. W. Visser, Biomixing of the oceans? Science **316**, 838 (2007).
[86] F. Blanchette, Mixing and convection driven by particles settling in temperature-stratified ambients, Int. J. Heat Mass Transfer **56**, 732 (2013).
[87] U. Frisch, *Turbulence: The Legacy of A. N. Kolmogorov* (Cambridge University Press, Cambridge, UK, 1995).
[88] N. Oakey and J. Elliot, Dissipation within the surface mixed layer, J. Phys. Oceanogr. **12**, 171 (1982).
[89] G. Sutherland, B. Ward, and K. Christensen, Wave-turbulence scaling in the ocean mixed layer, Ocean Sci. **9**, 597 (2013).
[90] P. A. Jumars, J. H. Trowbridge, E. Boss, and L. Karp-Boss, Turbulence-plankton interactions: A new cartoon, Mar. Ecol. **30**, 133 (2009).
[91] G. Piepke, A. Wüest, and D. C. Van Senden, Turbulent kinetic energy balance as a tool for estimating vertical diffusivity in wind-forced stratified waters, Limnol. Oceanogr. **45**, 1388 (2000).
[92] T. S. Lundgren, Linearly forces isotropic turbulence, technical report, Minnesota University, Minneapolis, MN, 2003 (unpublished).
[93] C. Rosales and C. Meneveau, Linear forcing in numerical simulations of isotropic turbulence: Physical space implementations and convergence properties, Phys. Fluids **17**, 095106 (2005).
[94] B. Cuenot, B. Bedat, and A. Corjon, NTMIX3D user's guide, preliminary version 1.0 (Centre de Recherche sur la Combustion Turbulente, France, 1997).
[95] T. Passot and A. Pouquet, Numerical simulation of compressible homogeneous flows in the turbulent regime, J. Fluid Mech. **181**, 441 (1987).